

# E- or Z-Isomers Arising from the Geometries of Ligands in the Mercury Complex of 2-(Anthracen-9-ylmethylene)-N-phenylhydrazine Carbothioamide

Jitendra Nath and Jubaraj B. Baruah\*

Cite This: *ACS Omega* 2023, 8, 42827–42839

Read Online

ACCESS |



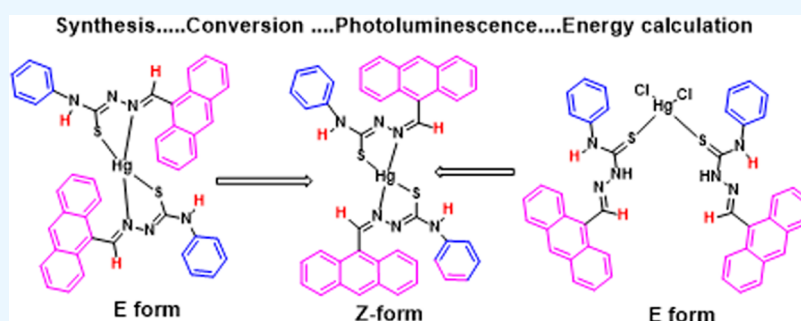
Metrics &amp; More



Article Recommendations



Supporting Information



**ABSTRACT:** An anionic mercury(II) complex of 2-(anthracen-9-ylmethylene)-N-phenylhydrazine carbothioamide (HATU) and two isomers of a neutral mercury(II) complex of the anion of the same ligand (ATU) were reported. The anionic complex  $[\text{Hg}(\text{HATU})_2\text{Cl}_2]\cdot\text{CH}_2\text{Cl}_2$  had a monodentate HATU ligand (a neutral form of the ligand) and chloride ligands. The two conformational isomers were of the neutral mercury(II) complex  $\text{Hg}(\text{ATU})_2\cdot 2\text{DMF}$ . The two isomers were from the *E* or *Z* geometry of the ligands across the conjugated  $\text{C}=\text{N}-\text{N}=\text{C}-\text{N}$  scaffold of the coordinated ligand. The two isomers of the complex were independently prepared and characterized. The spectroscopic properties of the isomers in solution were studied by  $^1\text{H}$  NMR as well as fluorescence spectroscopy. Facile conversion of the *E*-isomer to the *Z*-isomer in solution was observed. Density functional theory (DFT) calculations revealed that the *Z*-isomer of the complex was stable compared to the *E*-isomer by an energy of 14.35 kJ/mol; whereas, *E* isomer of the ligand was more stable than *Z* isomer by 8.37 kJ/mol. The activation barrier for the conversion of the *E*-isomer to the *Z*-isomer of the ligand was 167.37 kJ/mol. The role of the mercury ion in the conversion of the *E*-form to the *Z*-form was discussed. The mercury complex  $[\text{Hg}(\text{HATU})_2\text{Cl}_2]\cdot\text{CH}_2\text{Cl}_2$  had the *E*-form of the ligand. Distinct photophysical features of these mercury complexes were presented.

## INTRODUCTION

With the progress of time, new aspects of the isomers of metal complexes<sup>1</sup> are continuously emerging.<sup>1</sup> When the energy barrier between two conformers is above  $\sim 125$  kJ/mol, they are stable and isolable; these conformers may be considered under the category of isomers.<sup>1b,f</sup> The crystallographic studies on such isomers of inorganic complexes have been known since 1970.<sup>2a</sup> There are limited examples of such isomers of inorganic complexes.<sup>2</sup> In general, the energy barrier of conformers is low, and they easily get inter-converted in solution. In the solid state, some of them crystallize to be identified as conformational polymorphs, but they cannot be distinguished in solution under ordinary conditions.<sup>3</sup> Conformation polymorphs of inorganic complexes are prepared by crystallization from different solvents.<sup>4,5</sup> The characteristic color or emission features of the individual isomers<sup>6</sup> or polymorphs<sup>7</sup> of inorganic complexes provide impetus to understand them at the molecular level. Among these properties, aggregation-induced emission (AIE)<sup>8</sup> depends on

the geometry of ligands.<sup>9,10</sup> Thus, it is important to study the emission properties of different isomers of complexes where the fluorophore part of the ligand can be organized differently. A hydrazine carbothioamide-derived ligand, as represented in Figure 1, upon complex formation with metal ions would provide two isomers, as illustrated in Figure 1a,b. When  $R_1$  and  $R_2$  are chosen from dissimilar fluorophores, these isomers will have characteristic emission properties. Such complexes for comparative emission studies have not been studied so far, primarily because of their difficulties in synthesis in pure form.

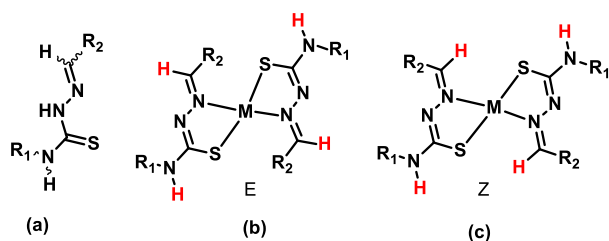
Received: August 7, 2023

Revised: September 30, 2023

Accepted: October 11, 2023

Published: October 31, 2023





$R_1$  and  $R_2$  are different substituent or functional groups; M = metal ion

**Figure 1.** (a) Representation of a hydrazine carbothioamide-derived ligand and (b) *E*- and (c) *Z*-isomers of the bis-chelated metal complex.

In this study, we have chosen 2-(anthracen-9-ylmethylene)-*N*-phenylhydrazine carbothioamide (**HATU**; when  $R_1$  = phenyl and  $R_2$  = anthracenyl in Figure 1a) as a ligand for the preparation of isomers of a mercury complex of the geometries illustrated in the Figure 1b,c. The chosen ligand has an anthracenyl fluorescent functional group, and in each of such proposed isomers, the ligands adopt  $\pi$ -conjugated structures and hence serve as model complexes for the study of the optical properties of such isomeric complexes. Alternatively, the anionic form (abbreviated **ATU**) of this, while serving as a ligand, adopts locked *E* or *Z* geometry through coordination to metal ions, and the anthracenyl group and the phenyl ring are positioned in *cis* or *trans* dispositions, respectively, with respect to each other across the C=N–N=C–N bond. We have chosen to study soft metal mercury complexes due to their ability to bind to sulfur as well as nitrogen to provide desired chelates. There are also examples of isomers,<sup>11</sup> polymorphs,<sup>12a</sup> and also mercury complexes with different conformations of ligands.<sup>12b</sup> The choice of the ligand is based on the extensive literature on thiosemicarbazide derivatives showing wide ranges of structures and the ability to form four coordinated complexes with structural variation.<sup>13</sup> Besides these, fluorescence modulation by such a ligand and also the detection of mercury ions have attracted interest for environmental remediation.<sup>14</sup> Anthracene-based compounds show emissions that are dependent on the geometrical arrangement of the anthracenyl groups in the solid state.<sup>16</sup> The mercury ion is well known to either quench or enhance the fluorescence emission of a ligand.<sup>15</sup> The ligand **HATU**<sup>15c</sup> is a fluorescent molecule, which was studied earlier as a probe for the detection of mercury ions and also preparation of copper and zinc complexes.<sup>11b</sup> So, to disclose the observation of different *E*- and *Z*-isomers from the orientations of the anthracenyl groups across a central metal ion, we explored such isomers and showed here their distinct characteristic signature in solid as well as in solution.

## EXPERIMENTAL SECTION

**General.** The infrared spectra of the solid samples were recorded with a PerkinElmer Spectrum Two Fourier transform infrared (FT-IR) spectrometer in the region of 4000–400  $\text{cm}^{-1}$  by using the ATR method. Powder X-ray diffraction patterns were recorded by using a Rigaku X-ray diffractometer where copper  $K\alpha$  ( $\lambda$  1.54 Å) was used as the source with 9 kW power.  $^1\text{H}$  NMR spectra were recorded on a BRUKER Ascend-600 MHz NMR spectrometer by using TMS as an internal standard. Thermogravimetry and DSC were carried out by using a thermal analyzer (STA449 F3 Jupiter) under argon with a heating rate of 10  $^\circ\text{C min}^{-1}$ . FESEM studies were

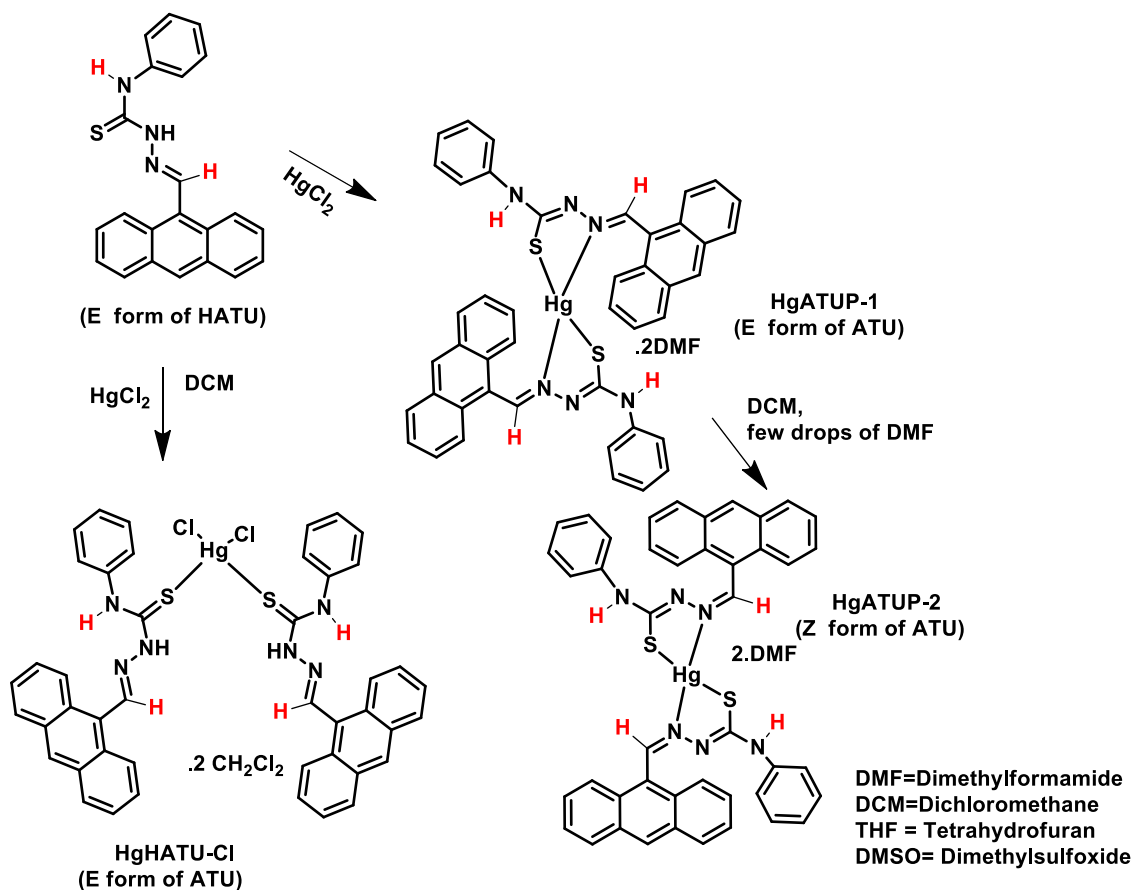
performed on a Gemini 300 FESEM instrument (Carl Zeiss) with samples prepared by placing  $\sim 2 \mu\text{L}$  of a 1 mM DMF solution by the drop-cast method on a glass plate covered with aluminum foil. The energy of the different assemblies and individual moieties were optimized, and the energy gaps between the highest occupied molecular orbital and the lowest unoccupied molecular orbital (HOMO–LUMO) were calculated by DFT using B3LYP/SDD. Fluorescence emissions were measured using a Horiba Jobin Yvon Fluoromax-4 Spectrofluorometer. Lifetime decay profiles were measured on an Edinburgh Instrument, Model: FSP920. The X-ray photoelectron spectroscopy (XPS) study was performed using a PHI 5000 Versa Probe III XPS system using monochromatic  $K\alpha$  radiation at a 1486.7 eV X-ray source. Elemental analyses were carried out on a 3000 series EuroEA elemental analyzer.

**Caution:** Mercury compounds are potentially hazardous; hence, experiments with them should be done in a fume hood and with adequate precautions.

**HgHATU-Cl.** A solution of the ligand (355 mg, 1 mmol) and mercury chloride (136 mg, 0.5 mmol) in dichloromethane (30 mL) was stirred at room temperature for 8 h. The precipitate was obtained in the case of methanol solvent, and there was a clear solution in the case of dichloromethane solvent. The yellow precipitate was dissolved in dichloromethane, and the solution was filtered and kept undisturbed for slow evaporation. After 1–2 days, the block crystal of **HgHATU-Cl** was obtained. Yield, 70%. IR (Neat,  $\text{cm}^{-1}$ ): 3250 (w), 3153 (w), 3038 (w), 2991 (w), 1624 (m), 1589 (m), 1546 (s), 1510 (s), 1451 (s), 1412 (w), 1349 (m), 1270 (s), 1206 (s), 1053 (s), 1022 (w), 952 (s), 935 (s), 910 (m), 888 (s), 841 (s), 783 (s), 759 (s), 723 (s), 695 (s), 637 (s), 591 (s), 557 (m), 497 (s), 485 (s), 454 (s), 420 (m).  $^1\text{H}$  NMR (600 MHz, dimethyl sulfoxide ( $\text{DMSO}$ )- $d_6$ , ppm): 12.13 (s, 2H), 10.13 (s, 2H), 9.45 (s, 2H), 8.74 (s, H–C=N, 2H), 8.58 (d, 4H), 8.16 (d,  $J$  = 8.4 Hz, 2H), 7.59–7.65 (m, 12H), 7.36 (t,  $J$  = 7.8 Hz, 4H), 7.19 (t, 2H), 5.75 (s, 2H).  $^{13}\text{C}$  NMR (125 MHz,  $\text{DMSO}$ - $d_6$ ): 174.55, 144.08, 138.69, 130.84, 130.69, 129.76, 128.96, 128.69, 128.25, 127.90, 127.36, 126.45, 125.61, 124.81, 53.52. Elemental analysis calculated for  $[\text{C}_{44}\text{H}_{34}\text{Cl}_2\text{HgN}_6\text{S}_2] \cdot \text{CH}_2\text{Cl}_2$  (**HgHATU-Cl**): C, 50.64; H, 3.40; N, 7.87; S, 6.01; found: C, 50.39; H, 3.33; N, 7.83; S, 6.05.

**HgATUP-1.** A solution of ligand **HATU** (355 mg, 1 mmol) and mercury chloride (136 mg, 0.5 mmol) in DMF (30 mL) was stirred at room temperature for 8 h. The resulting clear solution was filtered and kept undisturbed for slow evaporation. After 4–5 days, block-type crystals of **HgATUP-1** were obtained. Yield, 70%. IR (Neat,  $\text{cm}^{-1}$ ): 3385 (w), 3258 (w), 3049 (w), 1662 (s), 1595 (s), 1489 (s), 1430 (s), 1384 (w), 1308 (s), 1247 (s), 1178 (s), 1085 (s), 1062 (m), 1034 (w), 947 (m), 883 (s), 837 (s), 807 (m), 780 (w), 750 (w), 727 (s), 689 (s), 659 (s), 600 (w), 583 (s), 524 (m), 498 (s), 428 (s).  $^1\text{H}$  NMR (600 MHz,  $\text{DMSO}$ - $d_6$ , ppm): 9.19 (s, N–H), 8.57 (s, H–C=N–), 8.41 (s, N–H), 8.13 (d,  $J$  = 9 Hz, 4H), 7.95 (s, 2H), 7.95 (d,  $J$  = 8.4 Hz, 4H), 7.6 (t,  $J$  = 7.8 Hz, 4H), 7.51 (t,  $J$  = 7.8 Hz, 4H), 7.48 (d,  $J$  = 7.8 Hz, 4H), 7.26 (t,  $J$  = 7.2 Hz, 4H), 6.99 (t,  $J$  = 7.2 Hz, 2H), 2.89 (s, 6H).  $^{13}\text{C}$  NMR (125 MHz,  $\text{DMSO}$ - $d_6$ ): 162.39, 162.3, 151.27, 140.75, 130.86, 129.95, 129.16, 129.1, 128.05, 126.65, 126.09, 125.2, 124.63, 121.66, 120.59, 35.78, 30.77. Elemental analysis calculated for  $[\text{C}_{44}\text{H}_{32}\text{HgN}_6\text{S}_2] \cdot 2\text{C}_3\text{H}_7\text{NO}$  (**HgATUP-1**): C, 56.89; H, 4.39; N, 10.61; S, 6.07; found: C, 56.81; H, 4.36; N,

## Scheme 1. Preparation of Three Mercury Complexes



10.67; S, 6.09. ESI-MS: Calculated  $m/z$ - 911.1836; found:  $m/z$  911.2279 [(M + H)<sup>+</sup>, 100%].

**HgATUP-2.** A solution of ligand HATU (355 mg, 1 mmol) and mercury chloride (271 mg, 1 mmol) in DMF solvent (20 mL) was stirred at room temperature for 24 h. A yellow precipitate was obtained, which was dissolved in dichloromethane. The resulting solution was filtered, and 0.5 mL of DMF solvent was added to it and kept undisturbed for slow evaporation. After 2 days of standing, needle-type crystals of HgATUP-2 were obtained. Yield, 60%. IR (Neat, cm<sup>-1</sup>): 3254 (w), 3049 (w), 2919 (w), 2851 (w), 1664 (s), 1598 (s), 1532 (s), 1492 (s), 1432 (s), 1383 (m), 1310 (s), 1249 (s), 1184 (s), 1083 (s), 1064 (m), 1037 (m), 1014 (w), 953 (w), 938 (w), 887 (s), 840 (s), 809 (s), 781 (s), 756 (s), 725 (s), 690 (s), 658 (s), 606 (s), 585 (s), 519 (m), 494 (s). <sup>1</sup>H NMR (600 MHz, DMSO-*d*<sub>6</sub>, ppm): 9.57 (s, 2H), 8.73 (s, 2H), 8.69 (s, 2H), 8.16 (d, *J* = 8.4 Hz, 4H), 7.95 (s, 2H), 7.88 (d, *J* = 8.4 Hz, 4H), 7.48 (t, *J* = 7.2 Hz, 4H), 7.31 (t, *J* = 7.8 Hz, 4H), 6.80 (d, *J* = 7.8 Hz, 4H), 6.56 (t, *J* = 7.2 Hz, 2H), 6.46 (t, *J* = 7.8 Hz, 4H), 2.89 (s, 6H), 2.73 (s, 6H). <sup>13</sup>C NMR (125 MHz, DMSO-*d*<sub>6</sub>): 164.35, 162.3, 150.72, 140.16, 130.69, 129.52, 128.66, 127.94, 127.48, 126.34, 125.55, 125.5, 121.43, 120.55, 119.53, 35.78, 30.77. Elemental analysis calculated for [C<sub>44</sub>H<sub>32</sub>HgN<sub>6</sub>S<sub>2</sub>].2C<sub>3</sub>H<sub>7</sub>NO (HgATUP-2): C, 56.89; H, 4.39; N, 10.61; S, 6.07; found: C, 56.49; H, 4.33; N, 10.66; S, 6.13. ESI-MS: Calculated  $m/z$ - 911.1836; found:  $m/z$  911.2341 [(M + H)<sup>+</sup>, 100%].

**Crystallographic Study.** Single-crystal X-ray diffraction data were collected at 296 K with Mo K $\alpha$  radiation ( $\lambda$  = 0.71073 Å) by a Bruker Nonius SMART APEX CCD

diffractometer equipped with a graphite monochromator and an Apex CCD camera. Data reductions and cell refinement for a Bruker Nonius SMART APEX CCD diffractometer were performed using SAINT and XPREP software. Structures were solved by direct methods and refined by full-matrix least-squares on F<sup>2</sup> using SHELXL-2014 software. All non-hydrogen atoms were refined in anisotropic approximation against F<sup>2</sup> of all reflections. Hydrogen atoms were placed at their geometric positions by riding and refinement in the isotropic approximation. The crystal and refinement parameters are listed in Table S1 (Supporting Information). The solvent of the crystallization molecule present in HgHATU-Cl had high crystallographic disorder, while by refining the X-ray diffraction data, the disordered solvent was omitted by applying the squeeze command, and the squeezed solvent was confirmed to be dichloromethane by recording the NMR spectra and elemental analysis of HgHATU-Cl.

## RESULTS AND DISCUSSION

**Preparation of the Complexes.** The reactions of mercuric chloride with HATU depend on the solvents and the reaction conditions. Bis-chelated neutral with ATU or a monodentate cationic complex of mercury(II) with HATU was formed under different conditions, as shown in Scheme 1.

The reaction of HATU with mercuric chloride in dichloromethane yielded Hg(HATU)<sub>2</sub>Cl<sub>2</sub>. CH<sub>2</sub>Cl<sub>2</sub> (abbreviated HgHATU-Cl). The same reaction carried out in methanol yielded a yellow precipitate, which on recrystallization from dichloromethane provided HgHATU-Cl. The same reaction was performed in dimethylformamide; the pH of the solution

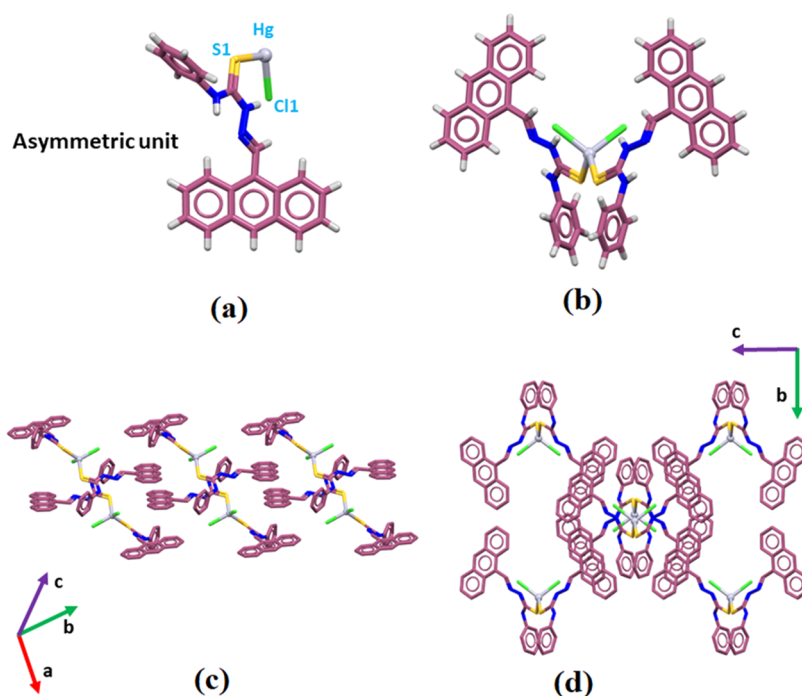


**Figure 2.** (a) Asymmetric unit, (b) crystal structure, (c) and (c, d) packing diagram of the complex drawn from two different views of complex HgHATU-Cl.

**Table 1. Metal–Ligand Bond Distances, Bond Angles, and  $\tau_4$  of HgATUP-1, HgATUP-2, and HgHATU-Cl Complexes**

complex	bond distance (Å)		bond angles (deg)			$\tau_4$ (geometry)
	Hg–X	Hg–S	X–Hg–X	S–Hg–S	X–Hg–S	
HgATUP-1	2.45, 2.48 <sup>a</sup>	2.36, 2.37	91.9 <sup>a</sup>	159.2	77.2, 76.9 <sup>a</sup>	0.77 (see-saw, $C_{2v}$ )
HgATUP-2	2.41, 2.44 <sup>a</sup>	2.37, 2.37	106.8 <sup>a</sup>	162.9	77.5, 78.2 <sup>a</sup>	0.64 (see-saw, $C_{2v}$ )
HgHATU-Cl	2, S2, 2.52 <sup>b</sup>	2.49, 2.49	104.6 <sup>b</sup>	105.3	108.9 <sup>b</sup>	0.97 ( $T_d$ )

<sup>a</sup>X = N. <sup>b</sup>X = Cl.

was changed from 5.3 to 1.27. This reaction in DMF within 3 h yielded the *E*-isomer of HgATUP-1. This suggested that the reaction released chloride by accepting the anionic form that is ATU, and hydrochloric acid was generated in solution. When the precipitate of HgATUP-1 was redissolved in dichloromethane with DMF and crystallized, it yielded the *Z*-isomer of HgATUP-2.

In the IR spectra, the N–H stretch of HgHATU-Cl appeared at 3250  $\text{cm}^{-1}$ . This peak was also observed in the isomers at a similar position (3254  $\text{cm}^{-1}$ ), whereas the C=S and C=N stretch of HgHATU-Cl appeared at 1451 and 1624  $\text{cm}^{-1}$ , respectively. These stretches appeared at 1430 and 1662  $\text{cm}^{-1}$  for the two isomers. The powder XRD of each complex was determined, and phase purity was ascertained by comparing the powder X-ray diffraction (PXRD) generated from the respective crystallographic information file. For this purpose, the PXRD patterns of the recrystallized samples of HgATUP-1 and HgATUP-2 were recorded independently and compared with crude products obtained under different conditions (Figures S6, S13, and S29). The thermogravimetry plots shown in Figure S22 showed four-step weight losses for both isomers. In thermogravimetry, the first step was the loss of weight due to the release of the DMF molecules, whereas the other three steps observed were from the weight loss from the ATU ligands. The weight losses from HgATUP-1 were observed at 144, 197, 318, and 380 °C; for HgATUP-2, these weight losses were at 135, 153, 204, 311, and 389 °C. These

weight losses were also reflected in the differential scanning calorimetry as four endothermic peaks from both isomers (Figure S22).

X-ray photoelectron spectroscopy (XPS) is a useful tool to discern the oxidation state as well as the environment around mercury ions.<sup>17</sup> The ionization potentials of the complexes determined by XPS are listed in Table S2. The two isomers could not be distinguished through XPS. Both showed <sup>4f</sup>Hg<sub>7/2</sub> and <sup>4f</sup>Hg<sub>5/2</sub> ionization energies as two peaks at 101.13 and 105.26 eV, respectively. On the other hand, HgHATU-Cl showed the characteristic ionization peaks for chloride. In this complex, the <sup>2p</sup>Cl<sub>1/2</sub> and <sup>2p</sup>Cl<sub>3/2</sub> ionization peaks were observed at 198.18 and 199.73 eV, respectively. <sup>2p</sup>S<sub>1/2</sub> and <sup>2p</sup>S<sub>3/2</sub> ionization peaks of the complex appeared in the region of 162.7–164.2 eV.

**Structural Aspects.** The crystal structure of complex HgHATU-Cl had a severely crystallographic disordered dichloromethane solvent, so the crystal structure of the dichloromethane solvate of Hg(HATU)<sub>2</sub>Cl<sub>2</sub> was refined by squeezing the dichloromethane part. The identity of the complex was ascertained by elemental analysis and by other spectral tools. It was a four-coordinate complex having two ligands and two chlorides (Figure 2) coordinated with a mercury ion to provide a four-coordinate complex. Depending on the type of ligands, mercury ions form mononuclear or polynuclear complexes of different geometries.<sup>13a18</sup> Also, the four-coordinate geometry of metal complexes may adopt an

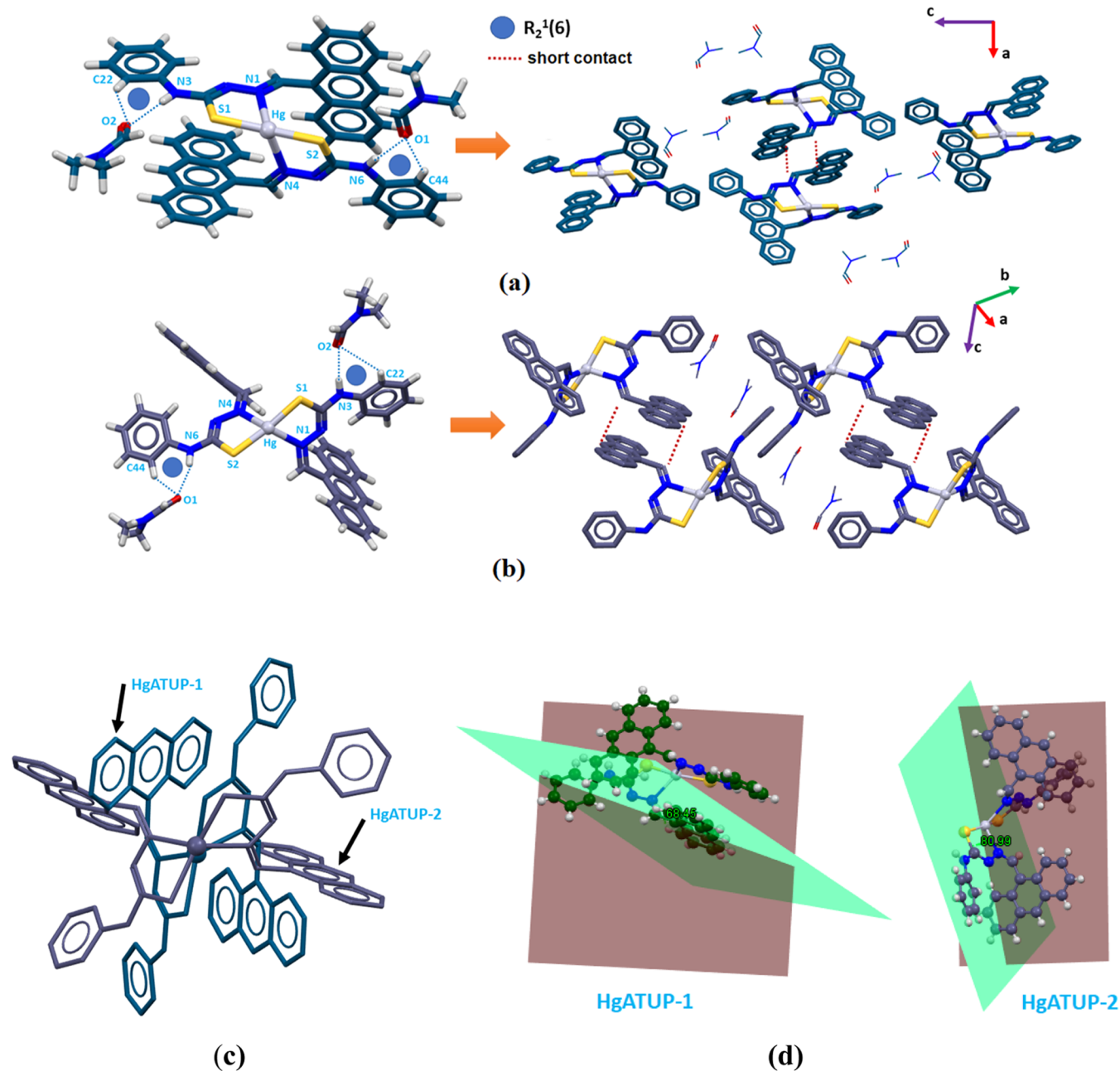


**Figure 3.** Structures and packing diagram of isomers (a) **HgATUP-1** and (b) **HgATUP-2**. (c) Overlaid structures of the two isomers (hydrogen atoms are omitted for clarity). (d) Angles between the planes containing the anthracenyl and phenyl rings of the same ligand in isomers **HgATUP-1** and **HgATUP-2**.

intermittent geometry between a tetrahedral structure and a square planar structure or a seesaw or trigonal bipyramid geometry. Thus, to clearly ascertain the geometry of the complex, the  $\tau_4$  parameter<sup>19</sup> of the complex was calculated by using the formula depicted in the literature, and it was found to be 0.967, which suggested a geometry around the mercury ion very close to a tetrahedron. The two Hg–S distances were equal to 2.49 Å; the Hg–Cl distances were 2.52 Å. The S–Hg–S, S–Hg–Cl, and Cl–Hg–Cl bond angles differed from the ideal tetrahedron (109.5°) between –4.1 and –0.6° (Table 1).

The structures of the *E*- and *Z*-isomers of the bis-chelated complex comprised two chelating ATU ligands bound to one four-coordinate mercury ion. Both had similar coordination

around the mercury (Figure 3a,3b) ion. The respective Hg–N and Hg–S bond distances and the S–Hg–S, N–Hg–S, and N–Hg–N bond distances are listed in Table 1. The Hg–S bonds in the two cases were similar, but there were differences in the Hg–N bond distances. The Hg–N bonds of **HgATUP-2** were slightly shorter (0.04–0.05 Å) than those of the other isomers. There were large differences in the orientations of the anthracenyl and phenyl groups in the isomers, as depicted in the overlaid geometry of the two isomers in Figure 3c. The differences in the orientations of the aromatic groups of the two isomers were revealed by drawing two independent planes, one containing the anthracenyl group and the other containing the phenyl group of the same ligand of the two isomers. The angle between these planes is illustrated in Figure 3d. Isomer

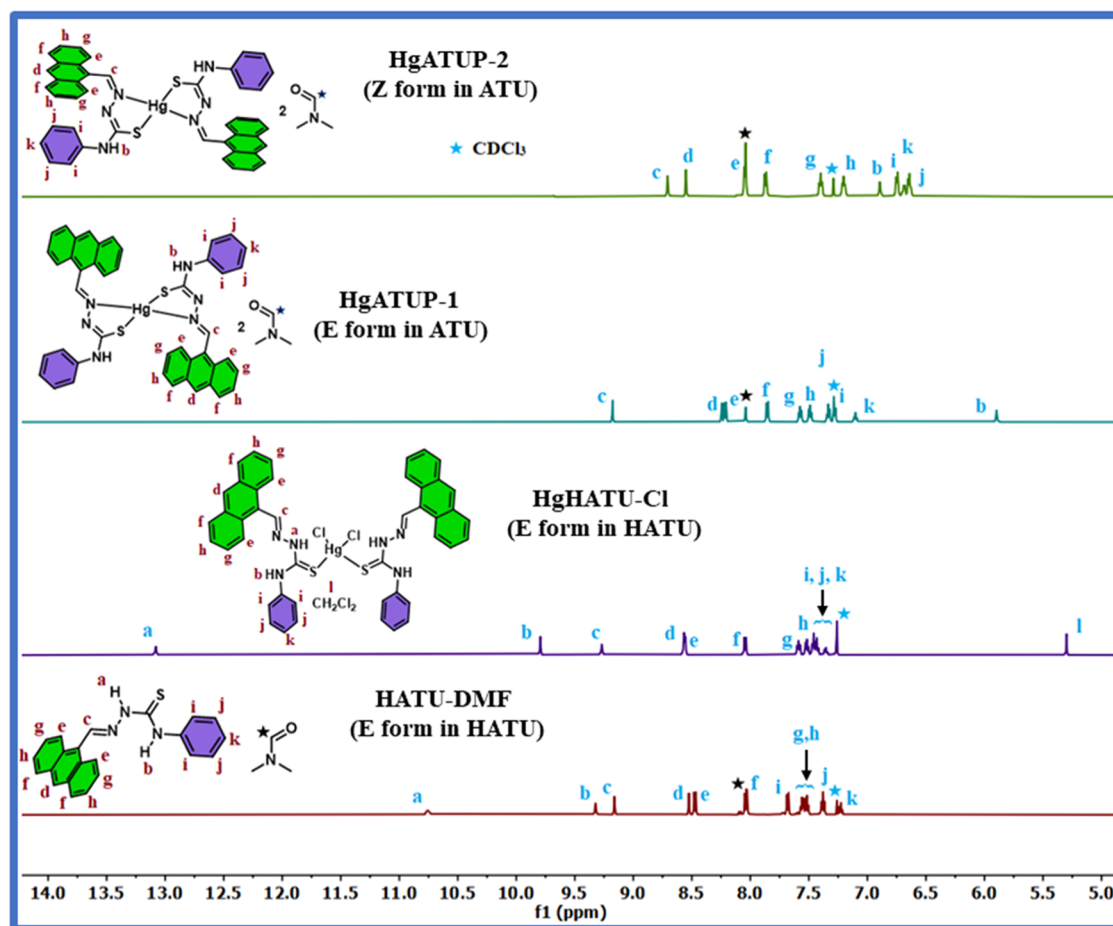


Figure 4.  $^1\text{H}$  NMR ( $\text{CDCl}_3$ , 600 MHz) of HATU-DMF, HgATUP-1, HgATUP-2, and HgHATU-Cl.

HgATUP-1 had a  $68.45^\circ$  angle between such planes, whereas, in HgATUP-2, it was  $80.89^\circ$ . For comparison, the angles between similar planes were evaluated for HATU and HgHATU-Cl, which were  $84.61$  and  $79.02^\circ$ , respectively. So, in the chloride complex, there was a change of  $5.59^\circ$  on the inter-planar angle as compared to that of the ligand, whereas the change in the angle in HgATUP-2 was  $3.72^\circ$ , but the same change in the angle in the isomer HgATUP-1 was  $-16.16^\circ$ . Thus, the orientations of the phenyl and anthracenyl groups of the ligand changed drastically in isomer HgATUP-1. To explain the propensity for the irreversible transformation of isomer HgATUP-1 to the other isomers, DFT calculations were carried out by optimizing the energy of each isomer. The total optimized energies of *Z*- and *E*-isomers were  $-3470.925$  and  $-3470.919$  hartree, respectively, which showed HgATUP-1 was more stable than HgATUP-2 by  $14.35$  kJ/mol. The stability difference between the *cis* and *trans* isomers is attributed to the steric and electronic requirements.

In a recent study, two conformational polymorphs of six-coordinate mercury piperonylate coordination polymers of the coligand 4,4'-bipyridine were reported.<sup>14a</sup> The activation barrier between the two conformers in that case was  $13.39$  kJ/mol; accordingly, a crystal-to-crystal transformation was possible. In the present case, we dealt with four-coordinate geometries where only solvent-assisted transformations were observed. As a consequence of the orientation difference, the packing patterns of the two isomers had large differences in the  $\pi$ -interactions; HgATUP-1 had dominant  $\text{N}-\text{H}\cdots\pi$  interac-

tions, whereas HgATUP-2 had extensive  $\text{C}-\text{H}\cdots\pi$  interactions, and in the latter case, anthracenyl groups were in the closer proximity with a centroid-to-centroid distance  $4.6$  Å. These aspects were also reflected in the electrostatic potential surfaces of the two isomers that were examined to understand the differences in the charged regions of the isomers (Figure S44). The Hirshfeld analysis<sup>20</sup> suggested the comparable weightages of the hydrophobic weak interaction schemes and also confirmed the presence of the  $\text{C}-\text{H}\cdots\pi$  and the  $\text{N}-\text{H}\cdots\pi$  interactions. The  $\text{N}-\text{H}\cdots\pi$  interactions have comparable magnitudes to the  $\text{C}-\text{H}\cdots\pi$  interaction and have energy values between  $4$  and  $20$  kJ/mol.<sup>21</sup> In the present case, the donor-acceptor distance varied from  $2.7$  to  $3.1$  Å, which was conventional in such compounds.<sup>21</sup> The parent ligand HATU crystallized as the DMF solvate, and its self-assembly was guided by homodimeric  $R_2^2(8)$  synthons built by two intermolecular  $\text{N}-\text{H}\cdots\text{S}$  hydrogen bonds. The DMF molecule was hydrogen bonded by the  $\text{N}-\text{H}$  next to the phenyl group with the  $\text{O}$  atom of DMF. It had extensive  $\pi$ -stacking between the anthracenyl groups. In this case, the anthracenyl groups of two neighboring molecules (Figure S23) were eclipsing each other and had a distance of separation of  $3.9$  Å. It had a one-dimensional chain-like arrangement.

**Conversion of Isomers in Solution Studied by  $^1\text{H}$  NMR Spectroscopy.** To probe the possible conversions of the complex and isomers in solution, the  $^1\text{H}$  NMR spectra of the isomers and HgHATU-Cl were examined under different conditions. The chemical shift positions of each complex were

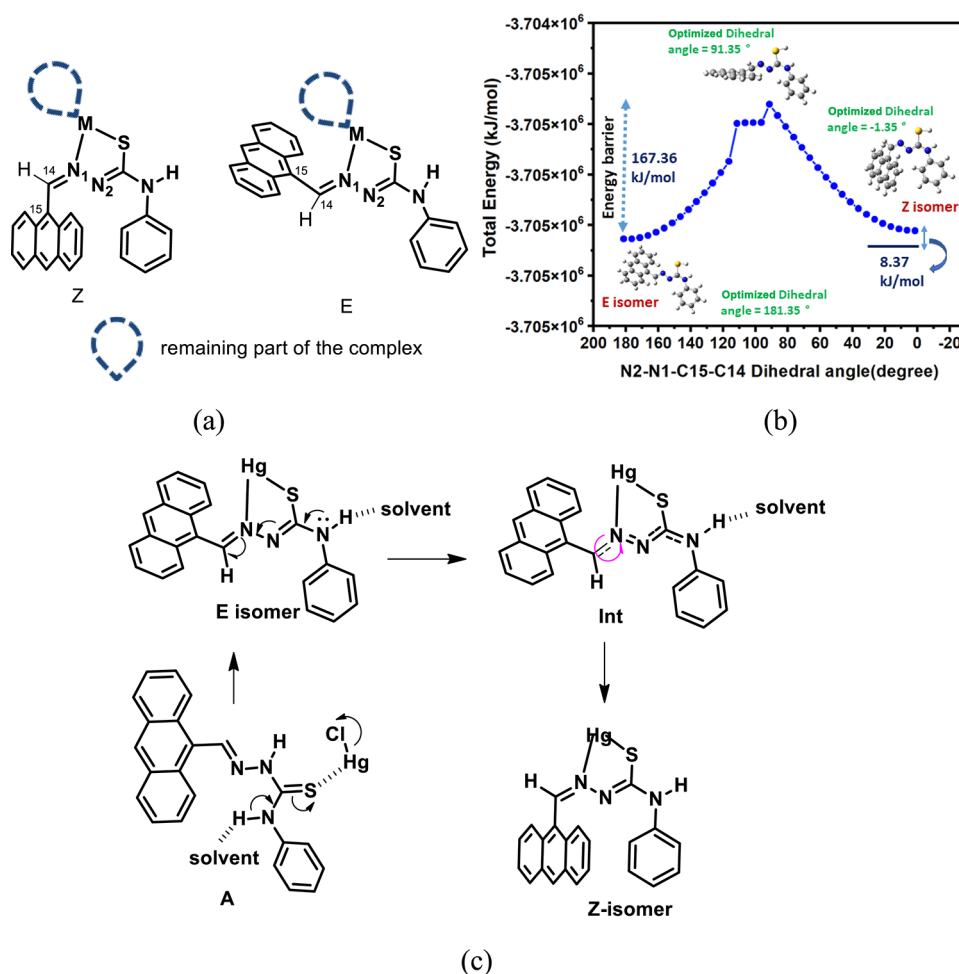


**Figure 5.** (a) Dihedral angle N2–N1–C15–C14 of the two isomers of the mercury complex. (b) The plot of DFT-calculated energy of the different orientations of **HATU** with respect to the change of every 5° of the dihedral angle N2–N1–C15–C14. (c) The plausible mechanism involving hydrogen bonds helping the conversion of the *E*-form to the *Z*-isomer and also formation of a bis-chelated complex from **HgHATU-Cl**.

solvent-dependent, and the peaks were shifted downfield as compared to the ligand. This is attributed to the diamagnetic effect of the mercury ion, contributing to the shielding. The  $^1\text{H}$  NMR spectra of the two isomers, **HgHATU-Cl**, and ligand **HATU** were recorded in  $\text{CDCl}_3$ . They are shown by including the assignment of each peak in Figure 4. The assignment of peaks was also done in the  $^1\text{H}$  NMR spectra recorded in the DMSO solution, as shown in Figure S30, and the spectra were found to be solvent-dependent. The 2D  $^1\text{H}$ -HOMO-COSY NMR spectra were recorded to confirm the assignments of the peaks (Figure S17).

The two isomers had large differences in their respective chemical shift positions, especially the  $\text{H}-\text{C}=\text{N}$  peak of **HgATUP-1** and **HgATUP-2**, which appeared as a singlet at 9.15 ppm and at 8.68 ppm in  $\text{CDCl}_3$ , respectively (peaks marked with blue stars in Figure 4). The aromatic peak marked as d of the anthracenyl group of **HgATUP-1** in  $\text{CDCl}_3$  appeared at 8.22 ppm, and for **HgATUP-2**, it appeared at 8.52 ppm. Clear distinction on the  $\text{N}-\text{H}$  chemical shifts of the complex **HgHATU-Cl**, as well as the isomeric complexes with the corresponding chemical shift of the free ligand, was observed. The respective  $\text{N}-\text{H}$  proton of the phenyl– $\text{N}-\text{H}$  of **HgATUP-1** and **HgATUP-2** appeared at 5.87 and 6.86 ppm in  $\text{CDCl}_3$ . Thus, the chemical shift of the proton of the phenyl– $\text{N}-\text{H}$  of **HgATUP-1** was more magnetically shielded than the

corresponding proton in **HgATUP-2**, which showed that the acidity of this proton was less in isomer **HgATUP-1**; alternatively, a higher negative character ( $\delta^-$ ) on this nitrogen atom was observed in **HgATUP-2**. This was a clear difference between the *Z*-isomer and the *E*-isomer. The phenyl– $\text{N}-\text{H}$  proton of **HgHATU-Cl** was shielded from the parent ligand and showed a decrease in the acidity of this  $\text{N}-\text{H}$  upon coordination of the ligand to the mercury ion. The proton of the  $\text{NH}-\text{C}=\text{S}$  part of **HgHATU-Cl** and the parent ligand were also at distinguishable positions; the former had this chemical shift at 13.25 ppm, whereas the chemical shift of the free ligand was at 10.75 ppm, which showed a higher acidity of  $\text{N}-\text{H}$  in the complex than that of the ligand. Thus, in the same solvent, the intrinsic acidity of the exchangeable protons of the complexes was different, suggesting that the geometry of the ligand together with the metal ion influences the intrinsic acidity of the labile  $\text{N}-\text{H}$  groups.

The  $\text{N}-\text{H}$  proton of the phenyl– $\text{N}-\text{H}$  of **HgATUP-1** and **HgATUP-2** appeared at 9.19 and 9.59 ppm, respectively, in  $\text{DMSO}-d_6$  (as shown in Figure S30). These lower values of the chemical shifts of the  $\text{N}-\text{H}$  protons in  $\text{CDCl}_3$  than that in the  $\text{DMSO}-d_6$  solvent were attributed to the lower basicity of  $\text{CDCl}_3$  than that of  $\text{DMSO}-d_6$ ; hence, the latter form strong hydrogen bonds eventually to deprotonate. The protons on the phenyl groups in both isomers displayed distinct chemical

shifts. The chemical shifts of the protons of the phenyl groups of **HgATUP-1** appeared at 7.08, 7.26, and 7.30 ppm in  $\text{CDCl}_3$ , whereas for **HgATUP-2**, these protons appeared at 6.61, 6.66, and 6.72 ppm in  $\text{CDCl}_3$ . Thus, the phenyl peaks were deshielded in **HgATUP-1** as compared to **HgATUP-2**. This was due to the different orientations of the neighboring aromatic anthracenyl groups affecting the magnetic field. The different orientations of the phenyl groups with respect to the anthracenyl groups is shown in Figure S25. The  $^1\text{H}$  NMR titrations in  $\text{DMSO}-d_6$  could delineate the formation of the complex of  $\text{HgCl}_2$  with the ligand. During titration, the chemical shifts of the N–H protons observed at 12.05 and 10.00 ppm from the ligands initially shifted (Figure S26) and finally disappeared due to the formation of **HgATUP-2**. The DMSO solvent has intrinsic basicity, hence allowed the deprotonation<sup>23</sup> of the active N–H proton from **HgATUP-2**. The  $^1\text{H}$  NMR of a solution of **HgHATU-Cl** in  $\text{DMSO}-d_6$  recorded at different time intervals revealed that the complex was less stable in solution and slowly transformed into **HgATUP-2**. It may be noted that the *E*-isomer **HgATUP-1** was less stable in solution and slowly transformed into **HgATUP-2**. The solution of **HgATUP-1** after 20 h in  $\text{DMSO}-d_6$  showed peaks of isomer **HgATUP-2** in  $^1\text{H}$  NMR spectra (Figure S27). All these transformations were examined by comparing the respective PXRD patterns of the isomers recovered from each solution and suggested that the respective signatures of the assemblies of the isomers in the solution were carried to the solid crystallized (Figure S29).

*E* or *Z* as depicted in Figure 5a was possible through a change in the N2–N1–C15–C14 dihedral angle in the isomers. This involves changes in the orientations across an extended delocalized C=N–N=C–N unit. The process does not require the dissociation of the ligand but requires a resonance structure of the chelating ligand, as illustrated in Figure 5c. It had to undergo change by having hydrogen bonds with solvent to permit the required rotation across the partial double bond. We could not carry out the calculation on energy variations with the different orientation changes in the respective isomers of the mercury complex, as there were two ligands in each complex. We calculated the energy changes of the *Z*-form of the thiol form of **HATU** transforming to the *E*-form through a DFT calculation on the energies of the ligand upon every  $5^\circ$  changes of the N2–N1–C15–C14 dihedral angle. The energy difference between the two isomers of the free ligand in the neutral form was found to be 8.37 kJ/mol (Figure 5b). This energy difference is comparable to the energy of a weak hydrogen bond or  $\pi$ -interaction. It was also found that the activation energy required to undergo conversion from the *E*- to *Z*-form of the neutral ligand (**HATU**) was 167.36 kJ/mol (Figure 5b). Based on the calculated activation barrier, the conversion of the *E*-isomer to the *Z*-isomer at ambient conditions<sup>1b</sup> would not have been possible without the assistance of hydrogen bonds of the ligand with a solvent. For such a conversion, a rotation across the C=N double bond is required. This could happen if the C15=N1 bond adopts a partial double bond character to undergo the rotation. We found that the pH of the respective solution of **HATU** (0.5 M) in DMF and DMSO solutions were 5.32 and 4.80, respectively, and the respective pH of these solutions changed to 1.02 and 2.15, respectively, upon addition of 2 mole equivalent of mercuric chloride. Whereas the pH of the solution of **HATU** ( $10^{-3}$  M) in chloroform was 3.20, it remained unchanged upon the addition of mercuric chloride in

the same ratio as in the other two solvents. The decrease in the pH in the respective DMF and DMSO solutions upon addition of mercury ions clearly showed that complexation passed through deprotonation. A mechanistic path involving hydrogen bonds with solvent for the formation of *Z*-isomer **HgATUP-1** or *E*-isomer **HgATUP-2** is illustrated in Figure 5c. In this figure, solvent molecules such as DMF formed hydrogen bonds with N–H, providing a partial C15=N1 character to allow the conversion of the isomers. A similar path is possible in the formation of isomers from complex **HgHATU-Cl**, which is also shown in Figure 5c, where the deprotonation, rotation, and chelation provided isomer of chelated complex.

**Implications of the Orientations of the Anthracenyl Group in Emission Spectra.** The anthracene-based mercury(II) complexes of tripodal ligands provide avenues to understand the emission mechanism.<sup>14b</sup> Having observed the isolable *E*- and *Z*-isomers of a chelated complex provided us with scope to understand their independent photophysical properties. The ultraviolet–visible (UV–vis) spectra of isomers **HgATUP-1** and **HgATUP-2** in chloroform showed absorption peaks at 396 and 389 nm, respectively (inset of Figure 6). Based on these absorption peaks, the optical band

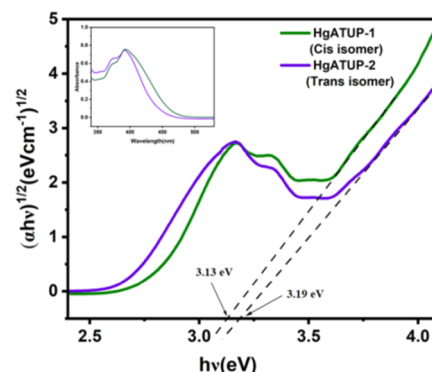


**Figure 6.** Tauc's plots showing the optical band gaps of the two isomers **HgATUP-1** and **HgATUP-2** {inset is the UV–vis spectra ( $10^{-6}$  M) of the two isomers in chloroform}.

gaps of the two isomers were ascertained by Tauc's plots<sup>23</sup> (Figure 6) and found to be 3.13 eV (396.1 nm) and 3.19 eV (388.7 nm) for *E*-isomer **HgATUP-1** and *Z*-isomer **HgATUP-2**, respectively. The DFT calculations by using the B3LYP/SDD basis set provided the HOMO–LUMO gaps 2.99 eV (414.7 nm) for **HgATUP-1** and 3.22 eV (385.0 nm) for **HgATUP-2** (Figure S43). Based on the DFT calculation, the absorption peaks were attributed to the HOMO-to-LUMO transitions. A similar fact was earlier observed in zinc complexes of the ligand.<sup>11b</sup> The absorptions were from ligand-based transitions and the slight difference in the positions of the absorptions of the *Z*- and *E*-isomers.

The *Z*-isomer (**HgATUP-2**) in chloroform showed emissions at 411, 436, and 462 nm ( $\lambda_{\text{ex}} = 380$  nm). These three peaks were due to the transition from the  $S_1$  to  $S_0$  state ( $\pi^*$ -to- $\pi$  transition) of the anthracenyl group, showing three peaks due to vibronic contributions. Peaks at similar places were observed for such a transition earlier in metal complexes having anthracenyl-based ligands.<sup>26a</sup> The position of the emissions of the *Z*-form in chloroform was unchanged upon dilution, but the intensity of each peak was enhanced (Figure 7a). This suggested that the isomer in a higher concentration in chloroform was in a fluorescence partial quenched state;

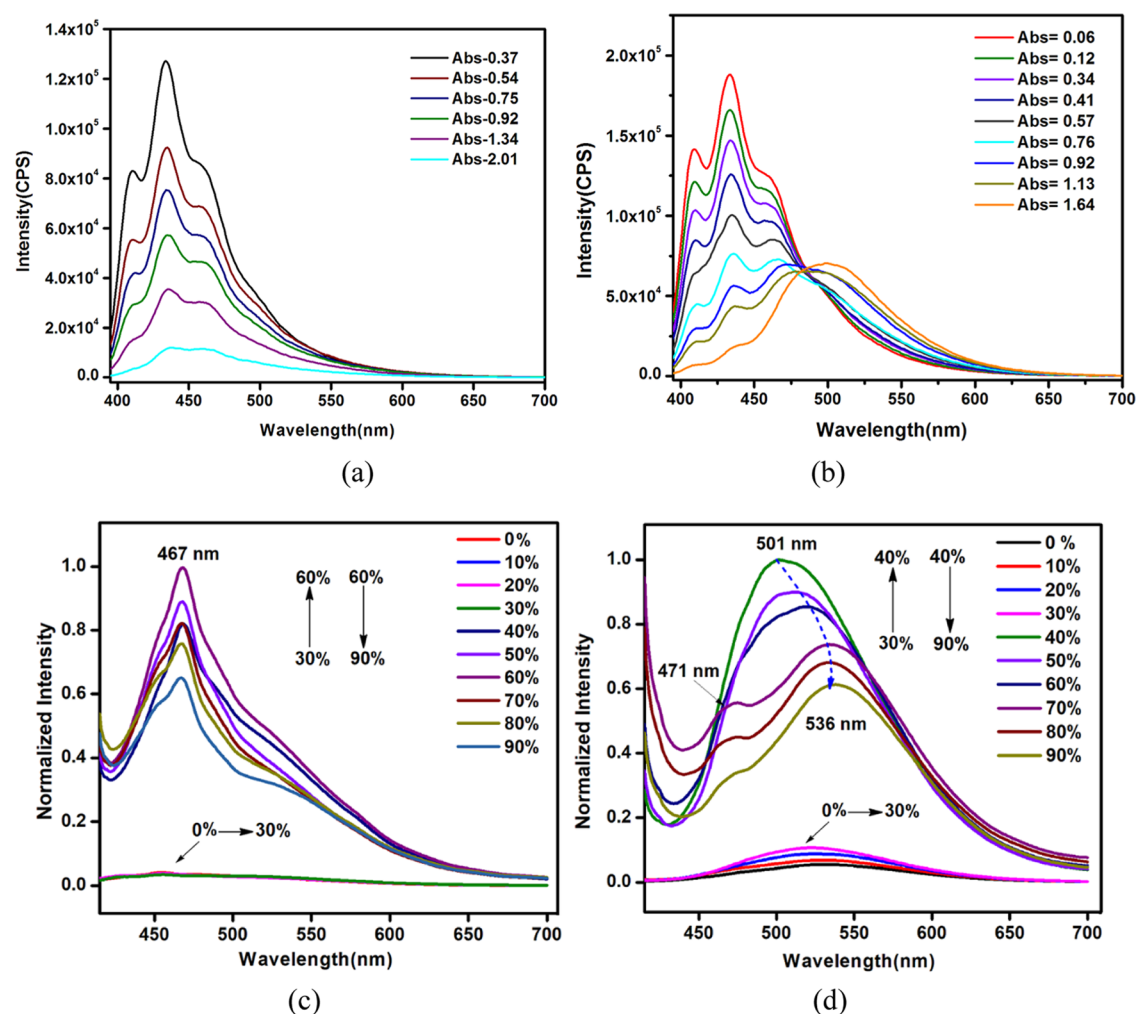


**Figure 7.** Changes in the fluorescence emission of (a) *E*-isomer **HgATUP-2** and (b) *Z*-isomer **HgATUP-1** at different molar concentrations in chloroform ( $\lambda_{\text{ex}} = 380$  nm,  $1.0 \times 10^{-8}$  to  $5 \times 10^{-7}$  M), Changes in the fluorescence emission ( $\lambda_{\text{ex}} = 400$  nm) of (c) *E*-isomer **HgATUP-2** and (d) *Z*-isomer **HgATUP-1** at different fractions of water in DMSO solution.

upon dilution, it disassembled. The crystal structure of the *Z*-isomer showed significant stacking and also N–H $\cdots\pi$  interactions. These contributed to the quenching of emissions. A concentration-dependent emission study of the *E*-isomer (**HgATUP-1**) in chloroform showed an excimer-like emission at 500 nm ( $\lambda_{\text{ex}} = 380$  nm). This emission was due to assembling, leading to eclipsing among the anthracenyl groups in the *E*-isomeric molecules. It may be noted that the anthracenyl group-containing complexes were reported earlier to have shown emission at 555 nm upon excitation at 365 nm, and this peak was assigned to excimer emission from  $\pi$ – $\pi$  interacting anthracene pairs.<sup>26ab</sup> Upon a decrease in the concentration of the isomer in chloroform, this emission (Figure 7b) diminished, and a new emission peak resembling the emission peaks of the *Z*-isomer was observed. The new peak was significantly enhanced upon further dilution. In the crystal structure of the *Z*-isomer, the anthracenyl groups were parallel but located at displaced positions. Upon dilution, the assembly was disassembled to show the property of discrete anthracenyl groups, and thereby, the emission intensity increased. In general, the  $\pi$ -stacking and Hg $\cdots\pi$  interactions quench the emission spectra of anthracene-based mercury complexes.<sup>15a</sup> In the present case, the two isomers have either N–H $\cdots\pi$  or C–H $\cdots\pi$  interactions. These interactions con-

tributed to the observed poor emissions from the isomers (Figure S46).

It is a practice to probe aggregation-induced emission by adding different amounts of water in an organic solvent.<sup>22</sup> We have carried out an emission study by having different fractions of water in the solution of the two isomers in a dimethyl sulfoxide (DMSO) solvent. A dimethyl sulfoxide solution of the *Z*-isomer (**HgATUP-2**) was also in a quenched state (Figure 7c), and no change in emission until 30% water was observed in the solution. But with an increasing amount of water from 30 to 60%, a peak developed at 467 nm. This peak resembles the *E*-isomer found in  $\text{CDCl}_3$ , attributing to the dilution effect and causing the disassembly of the isomer by water. The change in shape was a consequence of the differently aggregated form, where the vibrational contributions had changed. Beyond 60%, the emission decreased due to precipitation. The fluorescence emission of the *E*-isomer (**HgATUP-1**) in the DMSO solution was barely changed up to 30% water (initially, **HgATUP-1** was in a quenched state with a negligible emission at 503 nm; Figure 7d). Upon increasing the fractions of water up to 40 vol %, there was a sudden increase in the fluorescence intensity of the *E*-isomer, showing aggregation-induced enhancement. Between 40% and 90%, the fluorescence intensity was decreased due to

precipitation. The different geometry of functional groups of a fluorophore influences the aggregation-induced emissions.<sup>9</sup> On the other hand, chelation-induced emission contributes to the AIE of inorganic complexes.<sup>24</sup> The hydrogen bond plays an important role in the stabilization of the conformer of hydrazone derivatives,<sup>25</sup> and in our case, the aggregated state of the E-form was different from that of the Z-form, showing the difference in emission changes in each case.

The presence of a chloride ligand in an anthracene-based mercury complex can turn on the fluorescence emission of an anthracene unit.<sup>15b</sup> In HgHATU-Cl, there were no stacks among the anthracene rings, and the rings were oblique and at translated positions to each other, as there were no  $\pi$ -stacks among anthracene rings, showing feeble emission at 552 nm (Figure S46) in the solid state. In the solid state, free ligand HATU had extensive  $\pi$ -stacks (Figure S23a) among the anthracene rings with separation among the rings being 3.9 Å; hence, it was nonemissive. The long wavelength emissions in anthracenyl derivatives were usually attributed to aggregation-induced emission.<sup>16bc</sup> Complex HgHATU-Cl in chloroform showed a relatively strong emission at 506 nm ( $\lambda_{\text{ex}} = 380$  nm,  $\phi = 0.012$ ; Figure S33b) due to excimer emissions; this emission had the associated vibrational features. HATU and HgHATU-Cl showed a single exponential emission decay profile with short lifetimes of 0.151 and 0.152 ns, respectively. In general, the excimer emissions occurring from the anthracenyl excimer peak at around 500–550 nm generally have short lifetimes.<sup>ref</sup> The emission decay profiles monitored at 429 as well as at 456 nm in the DMSO solvent of the E-isomer showed biexponential behavior of their respective decay profiles. The average life-times of the emissions at these excitations were 6.84 and 4.45 ns, respectively. The emission decay at 528 nm in DMSO of Z-isomer HgATUP-1 was also biexponential, and it had an average lifetime of 2.77 ns. The solvent-dependent emission of palladium complexes having anthracenyl-derived ligands in dynamic equilibrium is known in the literature.<sup>26c</sup> The observation of the biexponential features from our E-form of the complex suggests the involvement of two emission paths in the E-isomers, that is, conventional  $\pi^*$ -to- $\pi$  transition and exciplex emission. Both the isomers showed short life-times involving exciplex emission, and the effect of the mercury ion was not directly felt by anthracene; a similar observation was earlier made in related systems.<sup>14b</sup>

## CONCLUSIONS

Due to the large activation barrier for the inter-conversion of E and Z geometry of the ligands across the conjugated C=N–N=C–N unit, two stable isomers of bis-chelated mercury(II) were observed. Those stable isomers in pure form could be selectively prepared from reactions carried out in the appropriate solvent. Energetically, the inter-conversion of the E-isomer to the Z-isomer of the parent ligand HATU is not favorable. Hence, the hydrogen bonding of the solvent to the mercury complex influenced the conversion by providing a partial double bond character to the C=N bond, allowing the change of the orientation of the phenyl or anthracenyl group. Conventionally, the E-isomer does not easily transform into the Z-isomer, but in the present circumstance, this was facile. The characteristic and distinct features of the respective isomers were shown through the <sup>1</sup>H NMR studies, and the distinct emission features arising from different orientations of the isomers could be shown. These examples established the

role of solvents in guiding the conversions of the complexes and rationally showed that the concentration of the complexes and the solvent significantly affect their optical properties. The E-isomer showed exciplex emission, whereas the Z-isomer showed conventional S<sub>1</sub>–S<sub>0</sub> emission. These data have further strengthened that the orientations of the fluorophores in a metal complex make a large difference in the position of peaks and intensity of respective emission spectra.

## ASSOCIATED CONTENT

### Supporting Information

The Supporting Information is available free of charge at <https://pubs.acs.org/doi/10.1021/acsomega.3c05806>.

Spectroscopic details; hirshfeld analysis; PXRD; FESEM images; XPS curves; TGA/DTG/DSC curves; electrostatic potential; hydrogen bond parameters; and HOMO–LUMO from DFT (PDF)

### Accession Codes

Crystallographic information files of the ligand and complexes were deposited to the Cambridge Crystallographic Database (CCDC numbers are 2233994, 2156292, 2156295, and 2156296)

## AUTHOR INFORMATION

### Corresponding Author

Jubaraj B. Baruah – Department of Chemistry, Indian Institute of Technology Guwahati, Guwahati 781 039 Assam, India; [orcid.org/0000-0003-3371-7529](https://orcid.org/0000-0003-3371-7529); Phone: +91-361-2582311; Email: [juba@iitg.ac.in](mailto:juba@iitg.ac.in)

### Author

Jitendra Nath – Department of Chemistry, Indian Institute of Technology Guwahati, Guwahati 781 039 Assam, India; [orcid.org/0000-0003-2862-8708](https://orcid.org/0000-0003-2862-8708)

Complete contact information is available at: <https://pubs.acs.org/doi/10.1021/acsomega.3c05806>

### Notes

The authors declare no competing financial interest.

## ACKNOWLEDGMENTS

The authors thank the Ministry of Education, Government of India, New Delhi, for grant No. F. No. 5-1/2014-TS.VII, North East Centre for Biological Sciences and Healthcare Engineering, Indian Institute of Technology Guwahati (project No. BT/COE/34/SP28408/2018) for the use of the SC-XRD facility (HgATUP-1 and HgATUP-2), and Department of Chemistry, Central Instrumentation facility of IIT Guwahati for general facilities.

## REFERENCES

- (1) (a) Moulton, B.; Zaworotko, M. J. From molecule to Crystal engineering: Supramolecular isomerism and polymorphism in network solids. *Chem. Rev.* **2001**, *101*, 1629–1658, DOI: [10.1021/cr9900432](https://doi.org/10.1021/cr9900432). (b) Rohmer, M.-M.; Bénard, M. Bond-stretch isomerism in strained inorganic molecules and in transition metal complexes: a revival? *Chem. Soc. Rev.* **2001**, *30*, 340–354. (c) Basilaia, M.; Chen, M. H.; Secka, J.; Gustafson, J. L. Atropisomerism in the pharmaceutically relevant realm. *Acc. Chem. Res.* **2022**, *55*, 2904–2919. (d) Salsman, J. C.; Kubiak, C. P.; Ito, T. Mixed valence isomers. *J. Am. Chem. Soc.* **2005**, *127*, 2382–2383. (e) Juraj, N. P.; Kirin, S. Inorganic stereochemistry: geometric isomerism in bis-tridentate ligand complexes. *Coord. Chem. Rev.* **2021**, *445*, No. 214051,

- DOI: 10.1016/j.ccr.2021.214051. (f) Pantazis, D. A.; McGrady, J. E. A three-state model for the polymorphism in linear tricoordinate compounds. *J. Am. Chem. Soc.* **2006**, *128*, 4128–4135. (g) Johnstone, T. C.; Lippard, S. J. Conformational isomerism of trans-[Pt(NH<sub>2</sub>C<sub>6</sub>H<sub>11</sub>)<sub>2</sub>L<sub>2</sub>] and the classical Wernerian chemistry of [Pt(NH<sub>2</sub>C<sub>6</sub>H<sub>11</sub>)<sub>4</sub>X<sub>2</sub> (X = Cl, Br, I)]. *Polyhedron* **2013**, *52*, 565–577, DOI: 10.1016/j.poly.2012.08.010. (h) Zhang, J.-P.; Huang, X.-C.; Chen, X.-M. Supramolecular isomerism in coordination polymers. *Chem. Soc. Rev.* **2009**, *38*, 2385–2396. (h) Zhang, J.-P.; Kitagawa, S. Supramolecular isomerism, framework flexibility, unsaturated metal center, and porous property of Ag(I)/Cu(I) 3,3',5,5'-tetramethyl-4,4'-bipyrazolate. *J. Am. Chem. Soc.* **2008**, *130*, 907–917.
- (2) (a) Jensen, K. G.; Solling, H.; Thorup, N. The crystal structure of two conformational isomers of meridional-trinitrito (ammine)-ethylenediaminecobalt(III) [Co(NO<sub>2</sub>)<sub>3</sub>NH<sub>3</sub>en]. *Acta Chem. Scand.* **1970**, *24*, 908–918. (b) Orthaber, A.; Karnah, M.; Tschierlei, S.; Streich, D.; Stein, M.; Ott, S. Coordination and conformational isomers in mononuclear iron complexes with pertinence to the [FeFe] hydrogenase active site. *Dalton Trans.* **2014**, *43*, 4537–4549. (c) Chen, D.-S.; Sun, L.-B.; Liang, Z.-Q.; Shao, K.-Z.; Wang, C.-G.; Su, Z.-M.; Xing, H.-Z. Conformational supramolecular isomerism in two-dimensional fluorescent coordination polymers based on flexible tetracarboxylate ligand. *Cryst. Growth Des.* **2013**, *13*, 4092–4099. (d) Zhang, G. -J.; Feng, G.; Xu, S.; Zhu, Z.; Lu, X.; Wu, J.; Liu, B. Structure dependent cis/trans isomerisation of terephenylene derivatives: consequences for aggregation induced emission. *Angew. Chem., Int. Ed.* **2016**, *55*, 6192–6196. (e) Wang, S.; Dormidontova, E. E. Tunable supramolecular networks via cis-trans metal–ligand isomerization. *Soft Matter* **2010**, *6*, 1004–1014. (f) Brittain, H. G.; Desreux, J. F. Luminescence and NMR studies of the conformational isomers of lanthanide complexes with an optically active polyaza polycarboxylic macrocycle. *Inorg. Chem.* **1984**, *23*, 4466–4469.
- (3) (a) Nangia, A. Conformational polymorphs in organic crystals. *Acc. Chem. Res.* **2008**, *41*, 595–604. (b) Cruz-Cabeza, A. J.; Bernstein, J. Conformational polymorphism. *Chem. Rev.* **2014**, *114*, 2170–2191.
- (4) Karmakar, A.; Sarma, R. J.; Baruah, J. B. Polymorphism in an aqua-bridged, dinuclear 2-nitrobenzoate complex of cobalt(II). *Eur. J. Inorg. Chem.* **2007**, *2007*, 643–647.
- (5) (a) Li, Z. H.; Xue, L. P.; Miao, S. B.; Zhao, B. T. Assembly of 4-, 6- and 8-connected Cd(II) pseudo-polymorphic coordination polymers: synthesis, solvent-dependent structural variation and properties. *J. Solid State Chem.* **2016**, *240*, 9–15. (b) Han, L.-L.; Hu, T.-P.; Mei, K.; Guo, Z.-M.; Yin, C.; Wang, Y.-X.; Zheng, J.; Wang, X.-P.; Sun, D. Solvent-controlled three families of Zn(II) coordination compounds: synthesis, crystal structure, solvent-induced structural transformation, supramolecular isomerism and photoluminescence. *Dalton Trans.* **2015**, *44*, 6052–6061.
- (6) Fleischauer, P. D.; Fleischauer, P. Photoluminescence of transition metal coordination compounds. *Chem. Rev.* **1970**, *70* (2), 199–223. (b) Alama, P.; Climent, C.; Alemany, P.; Laskar, I. R. Aggregation-induced emission” of transition metal compounds: design, mechanistic insights, and applications. *J. Photochem. Photobiol., C* **2019**, *41*, No. 100317, DOI: 10.1016/j.jphotochem.2019.100317. (c) de Segura, D. G.; Lalinde, E.; Moreno, M. T. Polymorphism and mechanochromism in 2-phenylbenzothiazole cyclometalated Pt<sup>II</sup> complexes with chelating NO ligands. *Inorg. Chem.* **2022**, *61*, 20043–20056, DOI: 10.1021/acs.inorgchem.2c03423. (d) Ni, J.; Zhang, X.; Qiu, N.; Wu, Y.-H.; Zhang, L.-Y.; Zhang, J.; Chen, Z.-N. Mechanochromic luminescence switch of platinum(II) complexes with 5-trimethylsilyl ethynyl-2,2'-bipyridine. *Inorg. Chem.* **2011**, *50*, 9090–9096. (e) Zhang, X.; Wang, J.-Y.; Qiao, D.; Chen, Z.-N. Phosphorescent mechanochromism through the contraction of Ag<sub>12</sub>Cu<sub>2</sub> clusters in tetradecanuclear copper-silver acetylide complexes. *J. Mater. Chem. C* **2017**, *5*, 8782–8787. (f) Kong, Y.-J.; Hu, J.-H.; Dong, X.-Y.; Si, Y.; Wang, Z.-Y.; Luo, X.-M.; Li, H.-R.; Chen, Z.; Zang, S.-Q.; Mak, T. C. W. Achiral-core-metal change in isomeric enantiomeric Ag<sub>12</sub>Ag<sub>32</sub> and Au<sub>12</sub>Ag<sub>32</sub> clusters triggers circularly polarized phosphorescence. *J. Am. Chem. Soc.* **2022**, *144*, 19739–19747. (g) Sivchik, V. V.; Grachova, E. V.; Melnikov, A. S.; Smirnov, S. N.; Ivanov, A. Y.; Hirva, P.; Tunik, S. P.; Koshevoy, I. O. Solid-state and solution metallophilic aggregation of a cationic [Pt(NCN)L]<sup>+</sup> cyclometalated complex. *Inorg. Chem.* **2016**, *55*, 3351–3363. (h) Yam, V. W.-W.; Au, V. K. -M.; Leung, S. Y. -L. Light-emitting self-assembled materials based on d<sup>8</sup> and d<sup>10</sup> transition metal complexes. *Chem. Rev.* **2015**, *115*, 7589–7728. (i) Tarai, A.; Baruah, J. B. Water-assisted emission enhancement of 2-hydroxynaphthaldoxime and related compounds. *ChemistrySelect* **2018**, *3*, 11406–11413. (j) Singh, M. P.; Tarai, A.; Baruah, J. B. Photo-physical properties of salts of a di-topic imidazole-tethered anthracene derivative in solid and solution. *CrystEngComm* **2019**, *21*, 4898–4909. (k) Alam, P.; Climent, C.; Kaur, G.; Casanova, D.; Choudhury, A. R.; Gupta, A.; Alemany, P.; Laskar, I. R. Exploring the origin of “Aggregation induced emission” activity and “Crystallization induced emission” in organometallic iridium(III) cationic complexes: influence of counter-ions. *Cryst. Growth Des.* **2016**, *16*, 5738–5752. (l) Peng, D.; He, L.-H.; Ju, P.; Chen, J.-L.; Ye, H.-Y.; Wang, J.-Y.; Liu, S.-J.; Wen, H.-R. Reversible mechanochromic luminescence of tetranuclear cuprous complexes. *Inorg. Chem.* **2020**, *59*, 17213–17223.
- (7) (a) Braga, D.; d'Agostino, S.; D'Amen, E.; Grepioni, F. Polymorphs from supramolecular gels: four crystal forms of the same silver(I) supergelator crystallized directly from its gels. *Chem. Commun.* **2011**, *47*, 5154–5156. (b) Vrdoljak, V.; Prugovecki, B.; Matkovic-Calogovic, D.; Hrenar, T.; Dreos, R.; Siega, P. Five *sra* topological Ln(III)-MOFs based on novel metal-carboxylate/Cl chain: structure, near-infrared luminescence and magnetic properties. *Cryst. Growth Des.* **2013**, *13*, 3773–3784. (c) Artemev, A. V.; Davydova, M. P.; Rakhmanova, M. I.; Bagryanskay, I. Y.; Pishchur, D. P. Family of Mn(II) complexes exhibiting strong photo- and triboluminescence as well as polymorphic luminescence. *Inorg. Chem. Front.* **2021**, *8*, 3767–3774. (d) Connick, W. B.; Henling, L. M.; Marsh, R. E.; Gray, H. B. Emission spectroscopic properties of the red form of dichloro(2,2'-bipyridine)platinum(II). Role of intermolecular stacking interactions. *Inorg. Chem.* **1996**, *35*, 6261–6265. (e) Schultz, A.; Li, X.; Barkakaty, B.; Moorefield, C. N.; Wesdemiotis, C.; Newkome, G. R. Stoichiometric self-assembly of isomeric, shape-persistent, supramacromolecular bowtie and butterfly structures. *J. Am. Chem. Soc.* **2012**, *134*, 7672–7675. (f) Meundaeng, N.; Rujiwatra, A.; Prior, T. J. Polymorphism in metal complexes of thiazole-4-carboxylic acid. *Transition Met. Chem.* **2016**, *41*, 783–793. (g) Sun, D.; Ke, Y.; Mattox, T. M.; Ooro, B. A.; Zhou, H.-C. Temperature-dependent supramolecular stereoisomerism in porous copper coordination networks based on a designed carboxylate ligand. *Chem. Commun.* **2005**, *43*, 5447–5449. (h) Sokolova, E. V.; Kinzhalov, M. A.; Smirnov, A. S.; Cheranyova, A. M.; Ivanov, D. M.; Kukushkin, V. Y.; Bokach, N. A. Polymorph-dependent phosphorescence of cyclometalated platinum(II) complexes and its relation to non-covalent interactions. *ACS Omega* **2022**, *7*, 34454–34462. (i) Liu, C.; Wang, C.; Sun, Z.-M. Conformational 2-fold interpenetrated uranyl supramolecular isomers based on (6,3) sheet topology: structure, luminescence, and ion exchange. *Inorg. Chem.* **2018**, *57*, 15370–15378.
- (8) (a) Mei, J.; Leung, N. L. C.; Kwok, R. T. K.; Lam, J. W. Y.; Tang, B. Z. Aggregation-induced emission: together we shine, united we soar! *Chem. Rev.* **2015**, *115*, 11718–11940. (b) Guan, J.; Shen, C.; Peng, J.; Zheng, J. What leads to aggregation-induced emission? *J. Phys. Chem. Lett.* **2021**, *12*, 4218–4226.
- (9) (a) Yang, H.; Zheng, J.; Xie, M.; Luo, D.; Tang, W.-J.; Peng, S.-K.; Cheng, G.; Zhang, X.; Zhou, X. -P.; Che, C.-M.; Li, D. Aggregation-enhanced emission in a red Cu(I) emitter with quantum yield > 99%. *ACS Mater. Lett.* **2022**, *4*, 1921–1928. (b) Gayathri, P.; Karthikeyan, S.; Pannipara, M.; Al-Sehemi, A. G.; Moon, D.; Anthony, S. P. Aggregation-enhanced emissive mechanofluorochromic carbazole-halogen positional isomers: tunable fluorescence via conformational polymorphism and crystallization-induced fluorescence switching. *CrystEngComm* **2019**, *21*, 6604–6612.
- (10) (a) Tang, M.-C.; Chan, M.-Y.; Yam, V. W.-W. Molecular design of luminescent gold (III) emitters as thermally vaporable and

- solvent-processable organic light-emitting device (OLED) materials. *Chem. Rev.* **2021**, *121*, 7249–7279. (b) Yan, L.-L.; Yao, L.-Y.; Yam, V. W.-W. Concentration- and solvation-induced reversible structural transformation and assembly of polynuclear gold (I) sulfido complexes. *J. Am. Chem. Soc.* **2020**, *142*, 11560–11568. (c) Tzeng, B.-C.; Lin, C.-Y.; Hung, J.-W.; Chen, S.-Y.; Chang, A. H. H.; Lee, G.-H. Solvent-induced luminescence and structural transformation of a dinuclear gold(I) (aza-18-crown-6)dithiocarbamate compound. *Inorg. Chem.* **2021**, *60*, 2694–2703. (d) Seki, T.; Ozaki, T.; Okura, T.; Asakura, K.; Sakon, A.; Uekusa, H.; Ito, H. Interconvertible multiple photoluminescence color of a gold(I) isocyanide complex in the solid state: solvent-induced blue-shifted and mechano-responsive red-shifted photoluminescence. *Chem. Sci.* **2015**, *6*, 2187–2195. (e) Ohno, K.; Hasebe, M.; Nagasawa, A.; Fujihara, T. Mechanochromic luminescence switch of platinum(II) complexes with 5-trimethylsilylethynyl-2,2'-bipyridine. *Inorg. Chem.* **2017**, *56*, 12158–12168.
- (11) Melnik, M. Isomers in the chemistry of mercury coordination compounds. *Cent. Eur. J. Chem.* **2010**, *8*, 469–485.
- (12) (a) Sánchez-Férez, F.; Solans-Monfort, X.; Calvet, T.; Font-Bardia, M.; Pons, J. Controlling the formation of two concomitant polymorphs in Hg(II) coordination polymers. *Inorg. Chem.* **2022**, *61*, 4965–4979. (b) Samie, A.; Sallimi, A. Conformational variation of ligands in mercury halide complexes; high and low Z' structures. *CrystEngComm* **2019**, *21*, 4951–4960.
- (13) (a) Arion, V. B. Coordination chemistry of S-substituted isothiosemicarbazides and isothiosemicarbazones. *Coord. Chem. Rev.* **2019**, *387*, 348–397. (b) Aguirre, A. R.; Parrilha, G. L.; Louro, S. R. W.; Alves, O. C.; Diniz, R.; Durval, F.; Rocha, W.; Beraldo, H. Structural and theoretical studies on copper(II) and zinc(II) complexes with a 9-anthraldehyde-derived thiosemicarbazone. *Polyhedron* **2022**, *217*, No. 115724, DOI: 10.1016/j.poly.2022.115724.
- (14) (a) Ding, S.-Y.; Dong, M.; Wang, Y.-W.; Chen, Y.-T.; Wang, H.-Z.; Su, C.-Y.; Wang, W. Thioether-based fluorescent covalent organic framework for selective detection and facile removal of mercury(II). *J. Am. Chem. Soc.* **2016**, *138*, 3031–3037. (b) Uritis, S.; Thummel, R. P.; Lee, H.-S.; Hancock, R. D. A study of the complexes of Hg(II) with polypyridyl ligands by Fluorescence, absorbance spectroscopy, and DFT calculations. The effect of ligand preorganization and relativistic effects on complex stability. *Inorg. Chim. Acta* **2022**, *530*, No. 120670, DOI: 10.1016/j.ica.2021.120670. (c) Cho, M.; Shin, H. J.; Kusumahastuti, D. K. A.; Yeo, H. K.; Min, S. Monomeric and tetrameric mercury(II) complexes with iodo and N2O2/N3O ligands: Structure and blue luminescence. *Inorg. Chim. Acta* **2020**, *511*, No. 119789, DOI: 10.1016/j.ica.2020.119789. (d) Tekuri, V.; Sahoo, S. K.; Trivedi, D. R. Hg<sup>2+</sup> induced hydrolysis of thiazole amine based Schiff base: Colorimetric and fluorogenic chemodosimeter for Hg<sup>2+</sup> ions in an aqueous medium. *Spectrochim. Acta, Part A* **2019**, *218*, 19–26. (e) Bai, C. B.; Qiao, R.; Liao, J. X.; Xiong, W. Z.; Zhang, J.; Chen, S.-S.; Yang, S. A highly selective and reversible fluorescence “OFF-ON-OFF” chemosensor for Hg<sup>2+</sup> based on rhodamine-6G dyes derivative and its application as a molecular logic gate. *Spectrochim. Acta, Part A* **2018**, *202*, 252–259. (f) Ghosh, S.; Alghunaim, A. S.; Al-mashhadani, M. H.; Krompiec, M. P.; Hallett, M.; Perepichka, I. F. 4,5-Diazafluorene co-oligomers as electron-deficient light-emitting materials and selective fluorescence sensors for mercury(II) cations. *J. Mater. Chem. C* **2018**, *6*, 3762–3773. (g) Vedamalai, M.; Kedaria, D.; Vasita, R.; Mori, S.; Gupta, I. Design and synthesis of BODIPY-clickate based Hg<sup>2+</sup> sensors: the effect of triazole binding mode with Hg<sup>2+</sup> on signal transduction. *Dalton Trans.* **2016**, *45*, 2700–2708. (h) Mikata, Y.; Nakanishi, K.; Nakagaki, F.; Kizu, A.; Konno, K. Off-on, ratiometric, and on-off fluorescence responses of thioether-linked bisquinolines toward Hg<sup>2+</sup> and Fe<sup>3+</sup> ions. *Eur. J. Inorg. Chem.* **2015**, *2015*, 3769–3780. (i) Saha, S.; Agarwalla, H.; Gupta, H.; Baidya, M.; Suresh, E.; Ghosh, S. K.; Das, A. New chemodosimetric probe for the specific detection of Hg<sup>2+</sup> in physiological condition and its utilisation for cell imaging studies. *Dalton Trans.* **2013**, *42*, 15097–15105. (j) Chethanakumar Budri, M.; Gudasi, K. B.; Vadavi, R. S.; Bhat, S. S. Luminescent pyrene-based Schiff base receptor for hazardous mercury(II) detection demonstrated by cell imaging and test Strip. *J. Fluoresc.* **2023**, *33*, 539–551. (k) Li, K.; Li, R.; Kong, X.; Shen, Q.; Wan, T.; Wu, H. A highly selective and sensitive fluorescent sensor based on a 1,8-naphthalimide with a Schiff base function for Hg<sup>2+</sup> in aqueous media. *Z. Naturforsch., B* **2022**, *77*, 611–617.
- (15) (a) Yoon, J.; Ohler, N. E.; Vance, D. H.; Aumiller, W. D.; Czarnik, A. W. A fluorescent chemosensor signalling only Hg(II) and Cu(II) in water. *Tetrahedron Lett.* **1997**, *38*, 3845–3848. (b) Lee, H.; Lee, H.-S.; Reibenspies, J. H.; Hancock, R. D. Mechanism of “Turn-on” fluorescent sensors for mercury(II) in solution and its implications for ligand design. *Inorg. Chem.* **2012**, *51*, 10904–10915. (c) Udhayakumari, D.; Velmathi, S.; Venkatesan, P.; Wu, S. P. Anthracene coupled thiourea as a colorimetric sensor for F<sup>-</sup>/Cu<sup>2+</sup> and fluorescent sensor for Hg<sup>2+</sup>/picric Acid. *J. Lumin.* **2015**, *161*, 411–416.
- (16) (a) Balasaravanan, R.; Siva, A. Synthesis, characterization and aggregation induced emission properties of anthracene based conjugated molecules. *New J. Chem.* **2016**, *40*, 5099–5106. (b) Densil, S.; Chang, C. H.; Chen, C. L.; Mathavan, A.; Ramdass, A.; Sathish, V.; Thanasekaran, P.; Li, W. S.; Rajagopal, S. Aggregation-induced emission enhancement of anthracene-derived Schiff base compounds and their application as a sensor for bovine serum albumin and optical cell imaging. *Luminescence* **2018**, *33*, 780–789. (c) Hu, J.; Lin, R.; Yip, J. H. K.; Wong, K.-Y.; Ma, D.-L.; Vittal, J. J. Synthesis and electronic spectroscopy of luminescent cyclometalated platinum-anthracenyl complexes. *Organometallics* **2007**, *26*, 6533–6543.
- (17) (a) Blackburn, J. R.; Nordberg, R.; Stevie, F.; Albridge, R. G.; Jones, M. M. Photoelectron spectroscopy of coordination compounds. Triphenylphosphine and its complexes. *Inorg. Chem.* **1970**, *9*, 2374–2376. (b) Louis, H.; Charlie, D. E.; Amodu, I. O.; Benjamin, I.; Gber, T. E.; Agwamba, E. C.; Adeyinka, A. S. Probing the reactions of thiourea (CH<sub>4</sub>N<sub>2</sub>S) with metals (X = Au, Hf, Hg, Ir, Os, W, Pt, and Re) anchored on fullerene surfaces (C<sub>59</sub>X). *ACS Omega* **2022**, *7*, 35118–35135.
- (18) (a) Drew, M. G. B.; McFall, S. G.; Nelson, S. M. Pentagonal pyramidal cadmium(II) and mercury(II) complexes of the quinque-dentate macrocyclic ligand 2,15-dimethyl-3,7,10,14,20-penta-azabicyclo[14.3.1] eicosa-1(20),2,14,16,18-pentaene. *J. Chem. Soc., Dalton Trans.* **1979**, *19*, 575–581. (b) Chieh, C.; Lee, L. P. C.; Chiu, C. Thiosemicarbazide complexes of mercury(II) halides. *Can. J. Chem.* **1978**, *56*, 2526–2531. (c) López-Torres, A.; Mendiola, M. A. Mercury complexes with the ligand benzaldehyde-N(4),N(4)-dimethylthiosemicarbazone. *Inorg. Chim. Acta* **2010**, *363*, 1275–1283.
- (19) Yang, L.; Powell, D. R.; Houser, R. P. Structural variation in copper(I) complexes with pyridylmethylamide ligands: structural analysis with a new four-coordinate geometry index  $\tau_4$ . *Dalton Trans.* **2007**, 955–964.
- (20) Spackman, M. A.; Jayatilaka, D. Hirshfeld surface analysis. *CrystEngComm* **2009**, *11*, 19–32.
- (21) (a) Nishio, M. The CH/π hydrogen bond in chemistry. Conformation, supramolecules, optical resolution and interactions involving carbohydrates. *Phys. Chem. Chem. Phys.* **2011**, *13*, 13873–13900. (b) Wang, J.; Yao, L. Dissecting C–H•••π and N–H•••π Interactions in two proteins using a combined experimental and computational approach. *Sci. Rep.* **2019**, *9*, No. 20149, DOI: 10.1038/s41598-019-56607-4. (d) Mukherjee, S.; Palit, S. R.; De, S. K. N–H•••π hydrogen bonding. *J. Phys. Chem. A* **1971**, *75*, 2404–2405. (e) Chantal, P. O.; Roman, P.; Leutwyler, L. S.; Bachoorz, R. A.; Klopfer, W. Strong N–H•••π hydrogen bonding in amide-benzene interactions. *J. Phys. Chem. B* **2009**, *113*, 2937–2943. (f) Kar, G. P.; Karmakar, A.; Baruah, J. B. N–H•••π interactions in two isomers of an amino group containing bis-phenol. *J. Chem. Crystallogr.* **2010**, *40*, 702–705.
- (22) Tarai, A.; Baruah, J. B. Conformation and visual distinction between urea and thiourea derivatives by an acetate Ion and a hexafluorosilicate cocrystal of the urea derivative in the detection of water in dimethylsulfoxide. *ACS Omega* **2017**, *2*, 6991–7001.

(23) Tauc, J.; Grigorovici, R.; Vancu, A. Optical properties and electronic structure of amorphous germanium. *Phys. Status Solidi B* **1966**, *15*, 627–663. (b) Makula, P.; Pacia, M.; Macyk, W. How to correctly determine the band gap energy of modified semiconductor photocatalysts based on UV–Vis spectra. *J. Phys. Chem. Lett.* **2018**, *9*, 6814–6817.

(24) (a) Alam, P.; Climent, C.; Alemany, P.; Laskar, I. R. Aggregation-induced emission” of transition metal compounds: design, mechanistic insights, and applications. *J. Photochem. Photobiol., C* **2019**, *41*, No. 100317, DOI: 10.1016/j.jphotochem.2019.100317. (b) Lim, N. C.; Schuster, J. V.; Porto, M. C.; Tanudra, M. A.; Yao, L.; Freake, H. C.; Brückner, C. Coumarin-based chemosensors for zinc(II): toward the determination of the design algorithm for CHEF-type and ratiometric probes. *Inorg. Chem.* **2005**, *44*, 2018–2030.

(25) Shao, B.; Baroncini, M.; Qian, H.; Bussotti, L.; Donato, M. D.; Credi, A.; Aprahamian, I. Solution and solid-state emission toggling of a photochromic hydrazone. *J. Am. Chem. Soc.* **2018**, *140*, 12323–12327.

(26) (a) Ma, X.-F.; Huang, X.-D.; Zheng, L.-M. Tuning the single-molecule magnet and photoluminescence properties of binuclear dysprosium complexes by light. *Cryst. Growth Des.* **2023**, *23*, 1095–1103. (b) Huang, X.-D.; Ma, X.-F.; Shang, T.; Zhang, Y.-Q.; Zheng, L.-M. Photocontrollable magnetism and photoluminescence in a binuclear dysprosium anthracene complex. *Inorg. Chem.* **2023**, *62*, 1864–1874. (c) Li, Y.; Rajasree, S. S.; Lee, G. Y.; Yu, J.; Tang, J.-H.; Ni, R.; Li, G.; Houk, K. N.; Deria, P.; Stang, P. J. Anthracene-triphenylamine-based platinum(II) metallacages as synthetic light-harvesting assembly. *J. Am. Chem. Soc.* **2021**, *143*, 2908–2919.